DELPHI 97-67 CONF 54
28 July, 1997

Angular Dependence of IR- and Collinear-Safe Shape Observables and a Precise Determination of α_S

Preliminary

DELPHI Collaboration

J. Drees, S. Hahn
Fachbereich Physik, Bergische Universität-GH Wuppertal
Gaußstraße 20, 42097 Wuppertal, Germany

Abstract

Using about 1.5 million events recorded with the DELPHI detector in 1994, a number of IR- and collinear-safe event shape observables are measured as a function of the polar angle ϑ_T of the thrust axis with respect to the e^+e^- beam direction. The data are compared to theoretical calculations in $\mathcal{O}(\alpha_s^2)$ including the event orientation.

A combined fit of α_s and of the renormalisation scale μ yields an excellent description of the high statistics data. Agreement with the data requires a rather narrow selection of the values of the renormalisation scale for each observable. For these scale values perfect consistency of the fit values of $\alpha_s(M_Z)$ is obtained for all event shape observables considered. A weighted average, taking into account correlations between the observables yields:

$$\alpha_S(M_Z^2) = 0.1164 \pm 0.0021.$$

Paper submitted to the LP'97 Conference
Hamburg, July 28 - August 1st

1 Introduction

The new attempt to perform a highly improved test of second order perturbation theory and to provide an improved measurement of $\alpha_S(M_Z^2)$ as presented in this paper is based on recent progress in next-to-leading order QCD calculations of oriented event shape distributions [1]. Furthermore the most recent DELPHI data used in this analysis are much improved both with respect to statistical and systematical accuracy as compared to previous DELPHI publications [3]. In total the distributions of 15 different infrared and collinear safe hadronic event observables are determined from 1.4 Million hadronic Z-decays at various values of the polar angle ϑ_T of the thrust axis with respect to the e^+e^-beam direction.

The precise experimental data are fully consistent with the expectation from second order QCD. For most of the distributions the renormalization scale must be fixed to a rather narrow range of values in order to describe the data. In earlier analyses using hadronic event shapes the renormalization scale was allowed to vary over a wide range in order to obtain consistent values of $\alpha_S(M_Z^2)$ from each of the investigated observables inside large "renormalization scale errors". Here a two parameter fit to each of the distributions measured at different ϑ_T intervals results in a fully consistent set of $\alpha_S(M_Z^2)$ values. The main errors of the 15 $\alpha_S(M_Z^2)$ values are therefore due to hadronization corrections and not to renormalization scale uncertainties. Any artificial increase of the error bars is avoided so that the degree of precision to which QCD can be tested remains transparent. In a final step an average value of $\alpha_S(M_Z^2)$ is derived taking account of the correlations between the values obtained from the different observables. In this way the maximum information is presented that can be inferred from experiment.

Since an important aspect of this study is the investigation of the dependence on the event orientation, no attempt is beeing made to include an α_S determination using the next-to-leading-log approximation of QCD (NLLA) for which the dependence on the event orientation would arise from matching with the investigated $\mathcal{O}(\alpha_s^2)$ calculation. Another main point of the present analysis consists in the quantitative comparison of the results on α_S obtained inside small errors from a large number of observables. Such a comparison is not possible in NLLA since calculations have been performed only for a limited number of distributions. It should also be remarked that additional uncertainties enter in NLLA analyses due to the unavoidable matching scheme ambiguities.

In section 2 the selection of hadronic events and the correction procedures applied to the data are briefly discussed. Section 3 introduces the investigated event shapes and describes the comparison to the expectations from various fragmentation models. Section 4 contains the comparison with angular dependent second order QCD and a detailed discussion of the QCD analysis performed. The results and their error bars are presented in section 5. The final results are summarized in the last section.

2 Selection of the Hadronic Events

2.1 Event Selection

In this analysis the reprocessed data measured with the DELPHI detector in 1994 at a center of mass energy of $\sqrt{s} = M_Z$ are used. Charged particles are selected if they fulfil the following criteria:

- momentum $p \geq 0.4 GeV/c$,
- $\Delta p/p \leq 1$,
- measured track length $l \geq 30$ cm,
- polar angle $20° \leq \theta_{Track} \leq 160°$,
- impact parameter with respect to the nominal interaction point within 4 cm perpendicular and 10 cm along the beam.

Hadronic events were selected if:

- There were at least 5 charged particles selected,
- the total charged energy $E_{charged} > 12\%\sqrt{S}$,
- the charged energy in each hemisphere of the detector, defined by the (x,y) plane $E_{hemis} > 3\%\sqrt{S}$,
- the polar angle of the thrust axis: $90.0° \leq \vartheta_T < 16.3°$.

In total about 1.4 million events satisfy these cuts. The selection efficiency is 92 %. Since the thrust axis does not distinguish between forward and backward directions, it is chosen such that $\cos\vartheta_T \geq 0$. ϑ_T is called the event orientation. The data are binned according to the event orientation into eight bins of $\cos\vartheta_T$ between 0.0 and 0.96. With the exception of the eighth bin, the thrust axis is well contained within the detector acceptance.

2.2 Correction Procedure

The contamination of beam gas events, $\gamma\gamma$ events and leptonic events other than $\tau^+\tau^-$, is expected to be less than 0.1 % and has been neglected. The influence of $\tau^+\tau^-$ events which have a pronounced 2-jet topology and contain high momentum particles has been determined by the KORALZ model [7] treated by the full simulation of the DELPHI detector DELSIM [6] and the standard data reconstruction chain. The $\tau^+\tau^-$ contributions have been subtracted from the measured data according to the relative abundance of $\tau^+\tau^-$ ($0.46\% \pm 0.03\%$) and hadronic events.

The observed data distributions were corrected for kinematic cuts, limited acceptance and resolution of the detector as well as effects due to reinteractions of particles inside the detector material. The correction for initial state photon radiation has been determined using events generated by JETSET 7.3 PS [8] with and without initial state radiation as predicted by DYMU3 [9]. The simulated data were processed in the same way as the real data. For an observable Y the a bin-by-bin correction factor $C(Y, \cos\vartheta_T)$ is calculated such as:

$$C(Y, \cos\vartheta_T) = \frac{\left(\frac{1}{\sigma}\frac{d^2\sigma}{dY\,d\cos\vartheta_T}\right)^{DELSIM}_{generated}}{\left(\frac{1}{\sigma}\frac{d^2\sigma}{dY\,d\cos\vartheta_T}\right)^{DELSIM}_{reconstructed}} \cdot \frac{\left(\frac{1}{\sigma}\frac{d^2\sigma}{dY\,d\cos\vartheta_T}\right)^{noISR}}{\left(\frac{1}{\sigma}\frac{d^2\sigma}{dY\,d\cos\vartheta_T}\right)^{ISR}} \tag{1}$$

Particles with a lifetime larger than 1 ns were considered as stable in the generated distributions. The bin widths were choosen on the basis the estimated experimental resolution so as to minimize bin-to-bin migration effects.

For the evaluation of systematic errors the cuts for the track- and event- selection were varied over a wide range, including additional cuts on the momentum imbalance, etc. From the stability of the measured distributions a systematic uncertainty has been computed as the variance with respect to the central value. As the systematic error is expected to grow proportional to the deviation of the overall correction factor from unity an additional relative systematic uncertainty of 10 % of this deviation has been added quadratically to the above value.

3 Measured Event Shapes and Comparison with Fragmentation Models

3.1 Definition of the Observables

Thrust T is defined by [15] :

$$T = \max_{\vec{n}_T} \frac{\sum_i |\vec{p}_i \cdot \vec{n}_T|}{\sum_i |\vec{p}_i|} \tag{2}$$

where $\vec{p}_i$ is the momentum vector of particle i, and $\vec{n}_T$ is the thrust axis to be determined.

Major M and Minor m are defined similarly, replacing $\vec{n}_T$ in the expression above by the Major axis $\vec{n}_{Maj}$, which maximizes the momentum sum transverse to $\vec{n}_T$ or the Minor axis $\vec{n}_{Min} = \vec{n}_{Maj} \times \vec{n}_T$ respectively.

The oblateness O is then defined by [16]:

$$O = M - m \tag{3}$$

The C-parameter C is derived from the eigenvalues λ of the infrared-safe linear momentum tensor $\Theta^{i,j}$ [17]:

$$\Theta^{i,j} = \frac{1}{\sum_k |\vec{p}_k|} \cdot \sum_k \frac{p_k^i p_k^j}{|\vec{p}_k|} \tag{4}$$

$$C = 3 \cdot (\lambda_1\lambda_2 + \lambda_2\lambda_3 + \lambda_3\lambda_1) \tag{5}$$

Events can be divided into two hemispheres, a and b, by a plane perpendicular to the thrust axis $\vec{n}_T$. With M_a and M_b denoting the invariant masses of the two hemispheres, the heavy jet mass ρ_H, light jetmass ρ_L, the sum of the jetmasses ρ_S and their difference ρ_L can be defined as

$$\rho_H = \frac{\max(M_a^2, M_b^2)}{E_{vis}^2} \tag{6}$$

$$\rho_L = \frac{\min(M_a^2, M_b^2)}{E_{vis}^2} \tag{7}$$

$$\rho_S = \rho_H + \rho_L \tag{8}$$

$$\rho_D = \rho_H - \rho_L \tag{9}$$

where E_{vis} is the total visible energy measured in a hadronic event.

Jet broadening measures have been proposed in [18]. In both hemispheres a and b the transverse momenta of the particles are added up, i.e. :

$$B_{a,b} = \frac{\sum_{i \in a,b} |\vec{p}_i \times \vec{n}_T|}{2 \sum_i |\vec{p}_i|} \tag{10}$$

The wide jet broadening B_{max}, the narrow jet broadening B_{min} , the total jet broadening B_{sum} and the difference of the jet broadening B_{dif} are then defined by

$$B_{max} = \max(B_a, B_b) \tag{11}$$

$$B_{min} = \min(B_a, B_b) \tag{12}$$

$$B_{sum} = B_{max} + B_{min} \tag{13}$$

$$B_{dif} = B_{max} - B_{min} \tag{14}$$

The first order prediction in perturbative QCD vanishes for both ρ_L and B_{dif}. Therefore these observables cannot be used for the determination of α_s.

Jet rates are commonly obtained using iterative clustering algorithms [19] in which a distance criterion or a metric y_{ij}, such as the scaled invariant mass, is computed for all pairs of particles i and j. The pair with the smallest y_{ij} is combined into a pseudoparticle (cluster) according to one of several recombination schemes. The clustering procedure is repeated until all of the y_{ij} are greater than a given threshold, the jet resolution parameter y_{cut}. The jet multiplicity of the event is defined as the number of clusters remaining, the n-jet rate $R_n(y_{cut})$ is the fraction of events classified as n-jet, and the differential two-jet rate is defined as

$$D_2(y_{cut}) = \frac{R_2(y_{cut}) - R_2(y_{cut} - \Delta y_{cut})}{\Delta y_{cut}} \tag{15}$$

Several algorithms have been proposed differing from each other in their definition of y_{ij} and their recombination procedure. We apply the E, $E0$, P, $P0$, JADE [20], Durham [21] and the Geneva algorithm [19]. The definitions of the metrics y_{ij} and the recombination schemes for the different algorithms is given below.

In the $E0$ algorithm y_{ij} is defined as the square of the scaled invariant mass of the pair of particles i and j:

$$y_{ij} = \frac{(p_i + p_j)^2}{E_{vis}^2} \tag{16}$$

while the recombination is defined by :

$$E_k = E_i + E_j \tag{17}$$

$$p_k = \frac{E_k}{|\vec{p}_i + \vec{p}_j|}(\vec{p}_i + \vec{p}_j) \tag{18}$$

where E_i and E_j are the energies and $\vec{p}_i$ and $\vec{p}_j$ are the momenta of the particles.

In the P algorithm y_{ij} is defined by Eq. (16), and the recombination is defined by

$$\vec{p}_k = \vec{p}_i + \vec{p}_j \tag{19}$$

$$E_k = |\vec{p}_k| \tag{20}$$

The $P0$ algorithm is defined analogue to the P algorithm, but the total energy E_{vis} is recalculated at each iteration according to

$$E_{vis} = \sum_i E_i \tag{21}$$

In the JADE algorithm, the definition of y_{ij} is

$$y_{ij} = \frac{2E_iE_j(1 - \cos\theta_{ij})}{E_{vis}^2} \tag{22}$$

where θ_{ij} is the angle between the pair of particles i and j. The recombination is defined by Eq. (19).

In the Durham algorithm, the recombination is also defined by Eq. (19), and

$$y_{ij} = \frac{2\min(E_i^2, E_j^2)(1 - \cos\theta_{ij})}{E_{vis}^2} \tag{23}$$

In the Geneva algorithm,

$$y_{ij} = \frac{8E_iE_j(1 - \cos\theta_{ij})}{9(E_i + E_j)^2} \tag{24}$$

with the recombination defined by Eq. (19).

The energy-energy correlation EEC [22] is defined in terms of the angle χ_{ij} between two particles i and j in an hadronic event:

$$EEC(\chi) = \frac{1}{N}\frac{1}{\Delta\chi}\sum_{N}\sum_{i,j}\frac{E_i E_j}{E_{vis}^2}\int\limits_{\chi-\frac{\Delta\chi}{2}}^{\chi+\frac{\Delta\chi}{2}} \delta(\chi' - \chi_{ij})d\chi' \qquad (25)$$

where N is the total number of events, $\Delta\chi$ is the angular bin width and the angle χ is taken from $\chi = 0°$ to $\chi = 180°$.

The asymmetry of the energy-energy correlation AEEC is defined as

$$AEEC(\chi) = EEC(180° - \chi) - EEC(\chi). \qquad (26)$$

The jet cone energy fraction JCEF [23] integrates the energy within a conical shell of an opening angle χ about the thrust axis. It is defined as

$$JCEF(\chi) = \frac{1}{N}\frac{1}{\Delta\chi}\sum_{N}\sum_{i}\frac{E_i}{E_{vis}}\int\limits_{\chi-\frac{\Delta\chi}{2}}^{\chi+\frac{\Delta\chi}{2}} \delta(\chi' - \chi_i)d\chi' \qquad (27)$$

where

$$\chi_i = \arccos\left(\frac{\vec{p}_i\vec{n}_T}{|\vec{p}_i|}\right) \qquad (28)$$

is the opening angle between a particle and the thrust axis vector $\vec{n}_T$, whose direction is defined here to point from the heavy jet mass hemisphere to the light jet mass hemisphere.

3.2 Fragmentation Models

QCD based hadronization models, which describe well the distributions of the event shape observables in the hadronic final state of e^+e^-annihilation, are commonly used for modelling the transition from the primary quarks to the hadronic final state. Perturbative QCD can describe only a part of this transition, the radiation of hard gluons or the evolution of a parton shower. For a determination of the strong coupling constant α_s one has to take account of the the so-called fragmentation or hadronization process, which is characterised by a small momentum transfer and hence a breakdown of perturbation theory. Several Monte Carlo models are in use to estimate the size of the hadronization effects and the corresponding uncertainty. The most frequently used fragmentation models, namely JETSET 7.3 PS [8], ARIADNE 4.06 [10] and HERWIG 5.8c [11] have been extensively studied and tuned to DELPHI data and to identified particle spectra from all LEP experiments in [4]. As discussed in detail in [4] [5] all models describe the data well. Examples of the measured hadron distributions are presented in figures 1 and 2. The increased systematical accuracy of the data is partially due to the fact that the ϑ_T dependence of the detector corrections is explicitely taken into account.

Before theoretical expressions describing parton distributions can be compared with experimental data, corrections have to be done for hadronization effects, i.e. effects resulting from the transition of the parton state into the observed hadronic state. For the

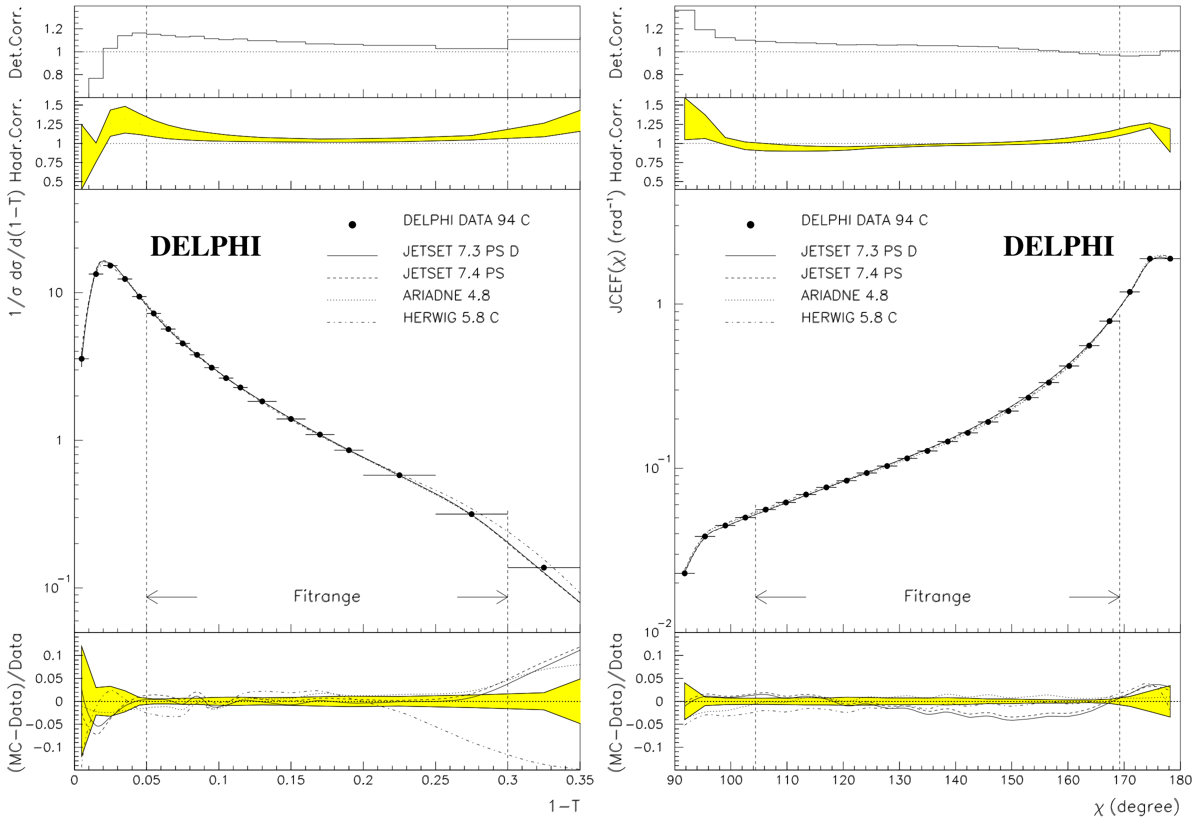

Figure 1: *left part:* Measured 1-T distribution integrated over $\cos\vartheta_T$. The upper part shows the detector correction including effects due to initial state radiation. The part below shows the size of the hadronization correction. The width of the band indicates the uncertainty of the correction. In the central part the measured 1-T distribution is compared to the expectation from four hadronization generators, JETSET 7.3 PS D with DELPHI modification of heavy particle decays, JETSET 7.4 PS, ARIADNE 4.8 and HERWIG 5.8 C. Also shown is the 1-T range used in the QCD fit. The lower part shows the ratio (Monte Carlo simulation-data)/data for the four hadronization generators. The width of the band indicates the size of the experimental errors.
right part: Same curves as shown in the left part but for JCEF integrated over $\cos\vartheta_T$.

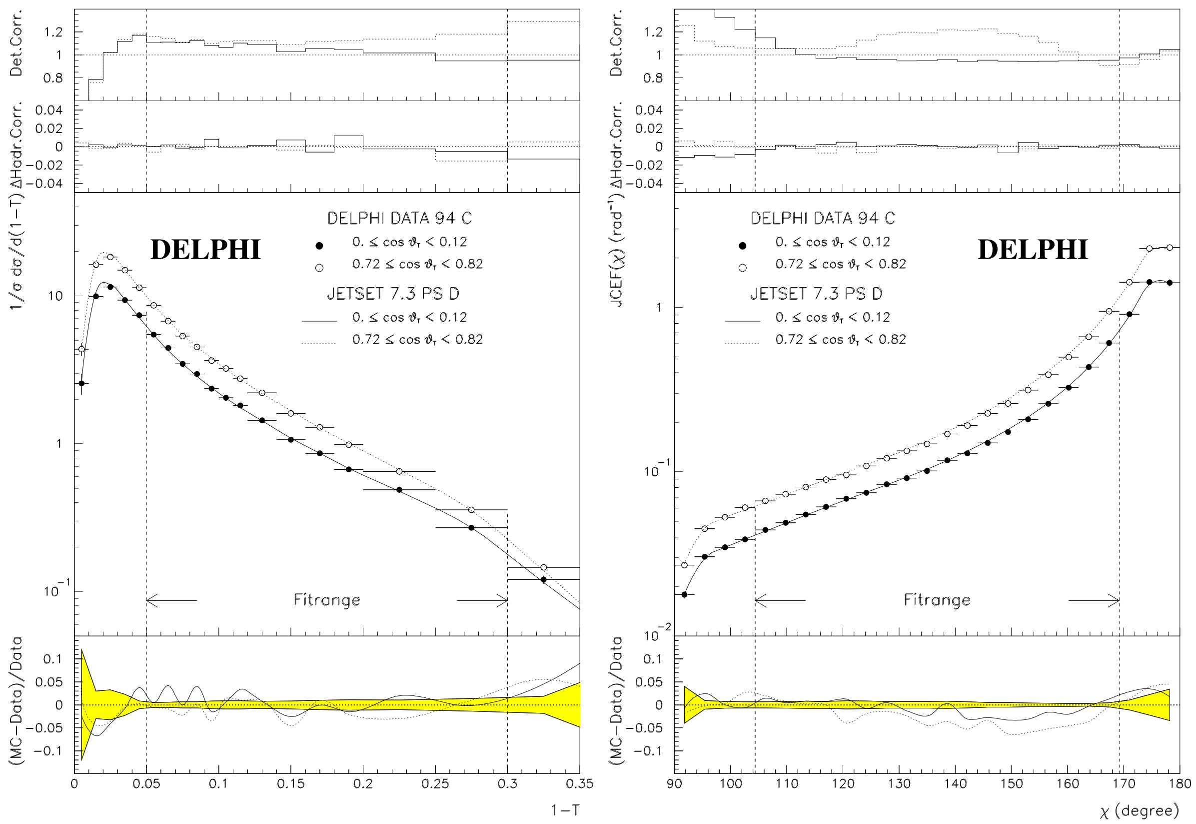

Figure 2: *left part:* Measured 1-T distribution in two bins of $\cos\vartheta_T$. The upper part shows the detector corrections in the two $\cos\vartheta_T$ bins. The part below shows the size of the relative hadronization correction in the two $\cos\vartheta_T$ bins with respect to the average correction. In the central part the measured 1-T distributions are compared to JETSET 7.3 PS D. The lower part shows the ratio (Monte Carlo simulation-data)/data for the two $\cos\vartheta_T$ bins.
right part: Same curves as shown in the left part but for JCEF in two bins of $\cos\vartheta_T$.

global event shape observables these transition is performed by a matrix P, where P_{ij} is the probability that a parton state contributing to the bin j of the partonic distribution will contribute to the bin i in the hadronic distribution as computed from the Monte Carlo model. This probability matrix has been applied to the distributions from $\mathcal{O}(\alpha_s^2)$ perturbative theory $D_{pert.}(Y, \cos\vartheta_T)$ to obtain the distributions for the predictions of the observed final state $D_{hadr.}(Y, \cos\vartheta_T)$:

$$D_{hadr.}(Y, \cos\vartheta_T)_i = \sum_j P_{ij}(Y, \cos\vartheta_T) D_{pert.}(Y, \cos\vartheta_T)_j \tag{29}$$

In the case of the $JCEF$, EEC and $AEEC$, which are defined in terms of single particles and pairs of particles, respectively, a bin-by-bin correction factor $C_{Hadr.}$ similarly to that described above for the detector effects have been computed such as:

$$D_{hadr.}(Y, \cos\vartheta_T)_i = C_{Hadr.}(Y, \cos\vartheta_T)_i D_{pert.}(Y, \cos\vartheta_T)_i \tag{30}$$

Our reference model for evaluating hadronization effects is the JETSET 7.3 Parton Shower (PS) Generator, which has been modified with respect to the heavy particle decays to obtain a better description of the heavy particle branching fraction. The tuned parameters have been taken from [4], where the updated tuning procedure is described in detail.

In order to estimate the systematic error of the hadronization correction the analysis is repeated using alternative Monte Carlo generators with different hadronization models. In addition the parameters for the JETSET PS have been varied. A description of the models and their differences can be found e.g. in [4]. The alternative models used are ARIADNE 4.06, HERWIG 5.8 c as well as version 7.4 PS JETSET PS model [8]. All these models have been tuned to DELPHI data [4]. For our standard Monte Carlo Program we applied also an alternative tuning to the DELPHI data [5] which includes Bose-Einstein correlations, not included in the reference tuning. Additionally the default setting of the JETSET PS parameter Q_0 has been varied, which controls the parton virtuality at which the PS is stopped. The Q_0 value was varied between $Q_0 = 0.5 GeV$ and $Q_0 = 4.0 GeV$. The systematic error of α_s originating from hadronization corrections is then estimated as the variance of the fitted α_s values obtained by using all hadronization corrections as mentioned above.

4 Comparison with Angular Dependent Second Order QCD

The evaluation of the $\mathcal{O}(\alpha_s^2)$ coefficients is performed by using EVENT2 [2], a program for the integration of the $\mathcal{O}(\alpha_s^2)$ matrix elements. The algorithm is described in [1].

Using this program, one can calculate the double differential cross section for any infrared- and collinear safe observable Y in e^+e^-annihilation in dependence on the event orientation:

$$\frac{1}{\sigma_{tot}}\frac{d^2\sigma(Y,\cos\vartheta_T)}{dY\,d\cos\vartheta_T} = \bar{\alpha_s}(\mu^2)\cdot A(Y,\cos\vartheta_T) + \bar{\alpha_s^2}(\mu^2)\cdot\Big[B(Y,\cos\vartheta_T) + \big(2\pi\beta_0\ln(x_\mu)-2\big)A(Y,\cos\vartheta_T)\Big] \quad (31)$$

where $\bar{\alpha_s} = \alpha_s/2\pi$ and $\beta_0 = (33-2n_f)/12\pi$. σ_{tot} is the one loop corrected cross section for the process $e^+e^- \to$ hadrons. The event orientation enters via ϑ_T, which denotes the polar angle of the thrust axis with respect to the e^+e^- beam direction. The renormalisation scale factor x_μ is defined by $\mu^2 = x_\mu Q^2$ where $Q = M_Z$ is the center of mass energy. A and B denote the $\mathcal{O}(\alpha_s)$ and $\mathcal{O}(\alpha_s^2)$ QCD coefficients, respectively.

Alternatively, the double differential cross section can be normalised to the partial cross section in each $\cos\vartheta_T$ interval:

$$R(Y,\cos\vartheta_T) := \frac{d\cos\vartheta_T}{d\sigma}\frac{d^2\sigma(Y,\cos\vartheta_T)}{dY\,d\cos\vartheta_T} \quad (32)$$

which is more appropriate for the study of the residual QCD effects.

The running of the strong coupling α_s at the renormalisation scale μ is in second order perturbative QCD expressed as

$$\alpha_s(\mu) = \frac{1}{\beta_0\ln\frac{\mu^2}{\Lambda^2}}\left(1 - \frac{\beta_1}{\beta_0^2}\frac{\ln\ln\frac{\mu^2}{\Lambda^2}}{\ln\frac{\mu^2}{\Lambda^2}}\right) \quad (33)$$

where $\Lambda \equiv \Lambda^{(5)}_{\overline{MS}}$ is the QCD scale parameter computed in the Modified Minimal Subtraction ($\overline{MS}$) scheme for $n_f = 5$ flavors and $\beta_1 = (153-19n_f)/24\pi^2$.

The renormalisation scale μ is a formally unphysical parameter and should not enter at all into an exact infinite order calculation [12]. Within the context of a truncated finite order perturbative expansion for any particular process under consideration, the definition of μ depends on the renormalisation scheme employed, and its value is in principle completely arbitrary. This renormalisation scale problem has been discussed extensively in the literature.

The traditional experimental approach to account for this problem has been to measure all observables at the same, fixed scale value, the so-called physical scale $x_\mu = 1$ or equivalently $\mu^2 = Q^2$. The scale dependence has been taken into account by varying μ over a wide range of values choosen within some ad hoc range, quoting the resulting change in the QCD predictions as theoretical uncertainty.

However, the approach of choosing $x_\mu = 1$ has a severe disadvantage. If we consider the ratio of the $\mathcal{O}(\alpha_s)$ and the $\mathcal{O}(\alpha_s^2)$ contributions, defined as

$$r(Y) := \frac{\alpha_s(x_\mu)\Big[B(Y) + A(Y)(2\pi\beta_0\ln(x_\mu)-2)\Big]}{A(Y)} \quad (34)$$

we find for many observables quite large values for the 2^{nd} order contibutions, in some cases this ratio is almost $|r(Y)| \simeq 1.0$, indicating a poor convergence behavior of the $\mathcal{O}(\alpha_s^2)$ predictions in the $\overline{MS}$ scheme which would quite naturally result in a wide spread of the measured α_s values which indeed has been observed in previous analysis in $\mathcal{O}(\alpha_s^2)$ QCD.

Several proposals have been made which resolve the problem by choosing optimized scales according to different theoretical prescriptions [13]. These methods have been discussed with some controversy [12] and till now no consensus has been achieved. Therefore, the only approach for determining an optimized scale value, which does not rely on specific theoretical assumptions is the experimental measurement of an optimized scale value μ for each measured observable seperately.

The procedure applied in this paper is a combined fit on α_s and the scale parameter x_μ. In the past this strategy suffered from a poor sensitivity of the fit with respect to x_μ for most of the observables. Due to the high statistics and high precision data now available, one may expect a better sensitivity at least for some of the observables under consideration.

We determined $\alpha_s(M_Z^2)$ and the renormalization scale factor x_μ simultaneously by comparing the corrected distributions for each observable Y with the perturbative QCD calculations corrected for hadronization effects as described in the previous section. The theoretical predictions have been fitted to the measured distributions $R(Y, \cos\vartheta_T)$ by minimizing χ^2, defined by using the sum of the squares of the statistical and systematic experimental errors, with respect to the variation of $\Lambda_{\overline{MS}}$ and x_μ.

The fit range has been chosen according to the following considerations:

- Requiring a detector acceptance larger than 80 %, the last bin in $\cos\vartheta_T$ has been excluded in general, i.e. the fit range has been restricted to the interval $0. \leq \cos\vartheta_T < 0.84$ which corresponds to the polar angle interval $32.9° < \vartheta_T \leq 90.0°$.
- Acceptance corrections have been required to be below about 25 % and the hadronization corrections to be below ~ 40 %.
- Following the naive expectation that a high ratio of the $\mathcal{O}(\alpha_s^2)$ contribution indicates a poor convergence behavior, we required the maximum contribution of the second order term over the whole fit range to be $r_{max}(Y) = \max|r(Y)| \leq 0.3$.
- The requirement that the data can be well described by the theoretical prediction, i.e. $\chi^2/d.f. \simeq 1.0$.
- Stability of the α_s - measurement with respect to the variation of the fit range.

The observables B_{sum}, B_{dif} and D_2^P could not satisfy the condition $r_{max} \leq 0.3$ for any fit range considered, therefore they have not been included in the further analysis steps.

4.1 Systematic and Statistical Uncertainties

For each observable the error on the combined determination of $\alpha_s(M_Z^2)$ and x_μ was defined by changing the parameters corresponding to an increase in χ^2 of 1.0 above the lowest value within the fit range defined above. In the case of asymmetric errors the higher value is taken. This error includes also the statistical uncertainties.

The experimental uncertainty was estimated by repeating the analysis with different selections to calculate the acceptance corrections as described in section 3. Additionally an analysis was performed, including neutral clusters measured with the hadronic or electromagnetic calorimeters. The overall uncertainty was taken as the variance of the individual $\alpha_s(M_Z^2)$ measurements.

An additional source of experimental uncertainty arises from the determination of the fit range, which has been estimated by varying the lower and the upper edge of the fit range by ± 1 bin, respectively, while the other edge is kept fixed. Half of the maximum deviation in $\alpha_s(M_Z^2)$ has been taken as the error due to the variation of the fit range and has been added in quadrature.

The hadronization uncertainty was determined as described in section 3. The total uncertainty on the $\alpha_s(M_Z^2)$ is determined from the sum of the squares of the errors listed above.

An underlying assumption for the $\mathcal{O}(\alpha_s^2)$ QCD fits to the shape observables is, that the renormalization scale is expected to be constant within the fit range. To check the importance of this assumption, a cross check for the differential two jet rate observables has been performed following a suggestion in [14]. For this observables the QCD fits have been repeated, allowing the renormalisation scale to vary proportional to y_{cut}, i.e. $\mu^2 = x_\mu y_{cut} \sqrt{S}$. The differences in the $\alpha_S(M_Z^2)$ determination have been found to be of the order of a few per mille for the individual jet rate observables and to be less than two per mille for the average of this observables.

5 Results

The results of the fits to 15 event shape distributions are summarised in tables 1 and 2 and shown in figure 3. The individual errors contributing to the total error of the α_S are listed in table 2.

More details concerning the QCD fits are presented in figures 4 to 10. Figures 4 and 5 show the values of $\alpha_S(M_Z^2)$ and the corresponding values of $\Delta\chi^2$ for the fits as a function of the scale $\lg(x_\mu)$ for all 15 investigated observables. The shape of the $\Delta\chi^2$ curves indicates that for most distributions the renormalization scale has to be fixed to a rather narrow range of values in order to be consistent with the data. Figures 6 to 10 contain a direct comparison of the data measured at various bins in $\cos\vartheta_T$ with the results of the QCD fits. Both, the measured dependence on $\cos\vartheta_T$ and on the studied observable are precisely reproduced by the fits.

Observable	Fit Range (Obs.)	Fit range ($\cos\vartheta_T$)	x_μ	χ^2/n_{df}
$1-T$	0.05 - 0.30	0.0 - 0.84	0.0034 ± 0.0002	1.24
O	0.24 - 0.44	0.0 - 0.84	1.76 ± 0.42	0.69
C	0.28 - 0.72	0.0 - 0.84	0.0047 ± 0.0004	1.23
B_{Max}	0.12 - 0.24	0.0 - 0.72	0.027 ± 0.014	0.96
ρ_H	0.03 - 0.30	0.0 - 0.84	0.0726 ± 0.0034	1.13
ρ_S	0.04 - 0.20	0.0 - 0.84	0.0104 ± 0.0006	1.01
ρ_D	0.01 - 0.30	0.0 - 0.84	1.15 ± 0.02	1.02
D_2^{E0}	0.05 - 0.20	0.0 - 0.84	0.113 ± 0.023	0.80
D_2^{P0}	0.05 - 0.20	0.0 - 0.72	0.075 ± 0.032	0.88
D_2^{Jade}	0.05 - 0.25	0.0 - 0.84	0.073 ± 0.014	0.85
D_2^{Durham}	0.02 - 0.12	0.0 - 0.84	0.0082 ± 0.0016	0.97
D_2^{Geneva}	0.07 - 0.14	0.0 - 0.84	0.11 ± 1.91	1.32
EEC	$28.8° - 158.4°$	0.0 - 0.84	0.0094 ± 0.0004	1.00
$AEEC$	$25.2° - 75.6°$	0.0 - 0.48	0.009 ± 0.028	0.70
$JCEF$	$104.4° - 169.2°$	0.0 - 0.84	0.0987 ± 0.0068	1.02

Table 1: Observables used in the $\mathcal{O}(\alpha_s^2)$ QCD fits. For each of the observables the fit range, the fit range in $\cos\vartheta_T$, the measured renormalisation scale factor x_μ together with the uncertainty as determined from the fit and the corresponding χ^2/n_{df} are shown.

Observable	$\alpha_S(M_Z^2)$	$\Delta\alpha_S$ (Fit)	$\Delta\alpha_S$ (Exp. syst.)	$\Delta\alpha_S$ (Hadr.)	$\Delta\alpha_S$ (Tot.)
$1-T$	0.1129	$\pm$ 0.0002	$\pm$ 0.0007	$\pm$ 0.0024	$\pm$ 0.0025
O	0.1171	$\pm$ 0.0014	$\pm$ 0.0015	$\pm$ 0.0054	$\pm$ 0.0058
C	0.1139	$\pm$ 0.0004	$\pm$ 0.0015	$\pm$ 0.0031	$\pm$ 0.0035
B_{Max}	0.1213	$\pm$ 0.0005	$\pm$ 0.0007	$\pm$ 0.0042	$\pm$ 0.0043
ρ_H	0.1204	$\pm$ 0.0003	$\pm$ 0.0017	$\pm$ 0.0027	$\pm$ 0.0032
ρ_S	0.1158	$\pm$ 0.0003	$\pm$ 0.0008	$\pm$ 0.0041	$\pm$ 0.0042
ρ_D	0.1150	$\pm$ 0.0004	$\pm$ 0.0015	$\pm$ 0.0062	$\pm$ 0.0064
D_2^{E0}	0.1183	$\pm$ 0.0005	$\pm$ 0.0010	$\pm$ 0.0023	$\pm$ 0.0026
D_2^{P0}	0.1207	$\pm$ 0.0005	$\pm$ 0.0015	$\pm$ 0.0056	$\pm$ 0.0058
D_2^{Jade}	0.1160	$\pm$ 0.0004	$\pm$ 0.0010	$\pm$ 0.0031	$\pm$ 0.0033
D_2^{Durham}	0.1173	$\pm$ 0.0006	$\pm$ 0.0008	$\pm$ 0.0025	$\pm$ 0.0027
D_2^{Geneva}	0.1190	$\pm$ 0.0040	$\pm$ 0.0011	$\pm$ 0.0045	$\pm$ 0.0061
EEC	0.1131	$\pm$ 0.0001	$\pm$ 0.0008	$\pm$ 0.0031	$\pm$ 0.0032
$AEEC$	0.1106	$\pm$ 0.0061	$\pm$ 0.0038	$\pm$ 0.0038	$\pm$ 0.0081
$JCEF$	0.1163	$\pm$ 0.0001	$\pm$ 0.0007	$\pm$ 0.0025	$\pm$ 0.0026

Table 2: Individual sources of errors of the $\alpha_S(M_Z^2)$ measurement. For each observable, the value of $\alpha_S(M_Z^2)$, the uncertainty from the fit, the systematic experimental uncertainty, the uncertainty resulting from hadronization corrections and the total uncertainty are shown.

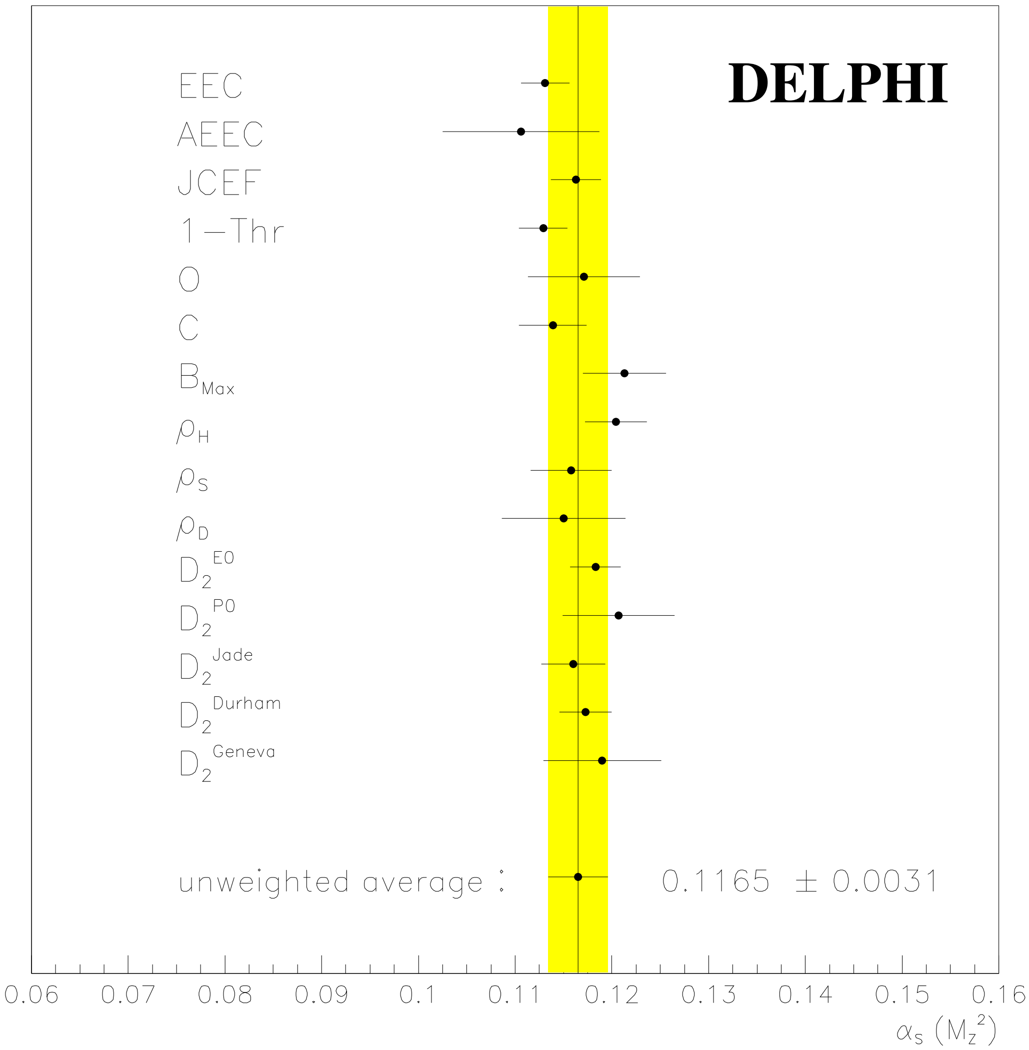

Figure 3: Results of the fits of 15 event shape distributions. Also shown is the unweighted average.

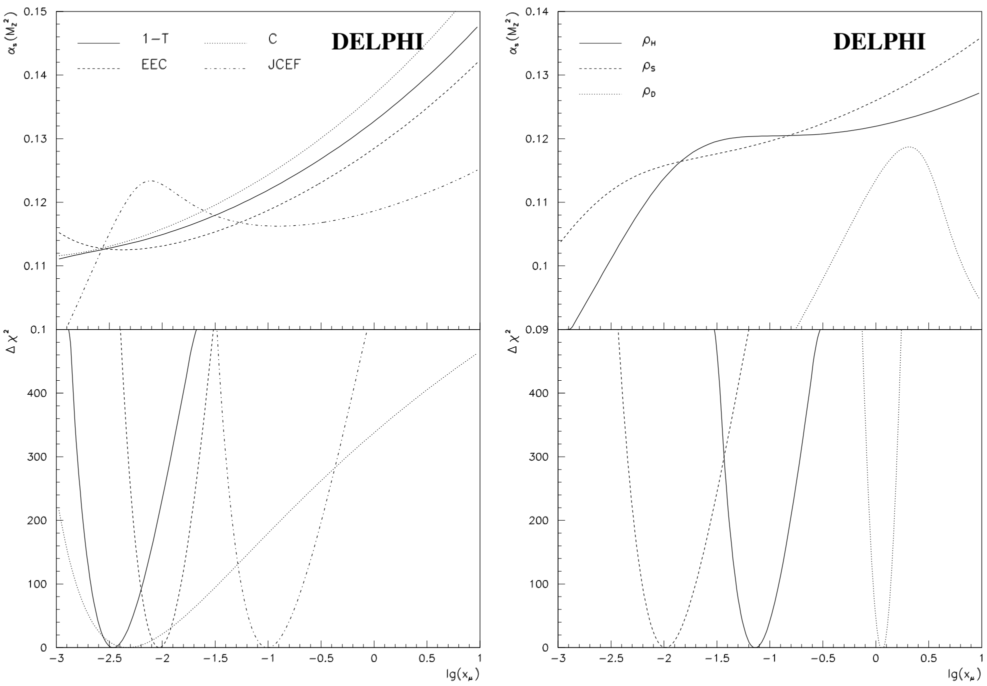

Figure 4: $\alpha_S(M_Z^2)$ and $\Delta\chi^2 = \chi^2 - \chi^2_{min}$ from $\mathcal{O}(\alpha_s^2)$ fits to the double differential distributions in $\cos\vartheta_T$ and $1-T$, C, EEC, $JCEF$, ρ_H, ρ_S, ρ_D .

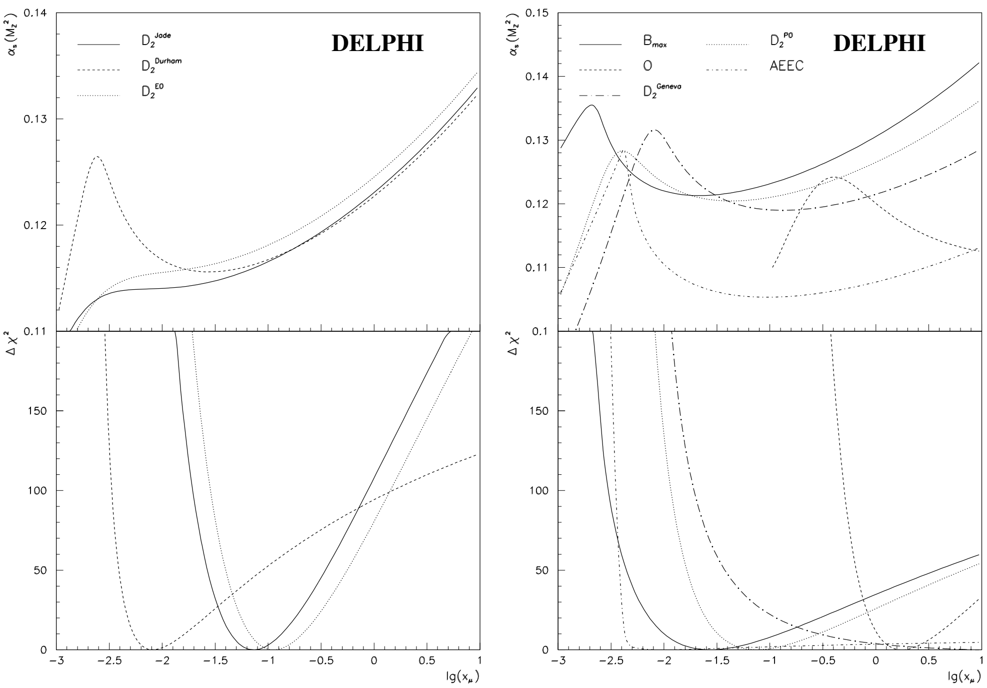

Figure 5: $\alpha_S(M_Z^2)$ and $\Delta\chi^2 = \chi^2 - \chi^2_{min}$ from $\mathcal{O}(\alpha_s^2)$ fits to the double differential distributions in $\cos\vartheta_T$ and D_2^{Jade}, D_2^{Durham}, D_2^{E0}, D_2^{P0}, D_2^{Geneva}, B_{max}, $Oblateness$, $AEEC$
.

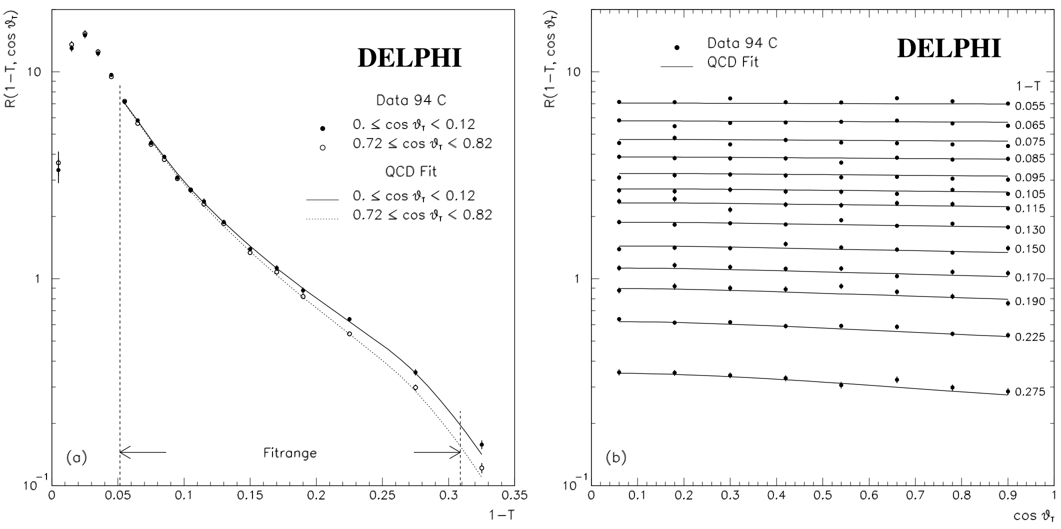

Figure 6: (a) QCD fits to the measured thrust distribution for two bins in $\cos\vartheta_T$. (b) Measured thrust distribution at various fixed values of $1-T$ as a function of $\cos\vartheta_T$. The solid lines represent the QCD fit.

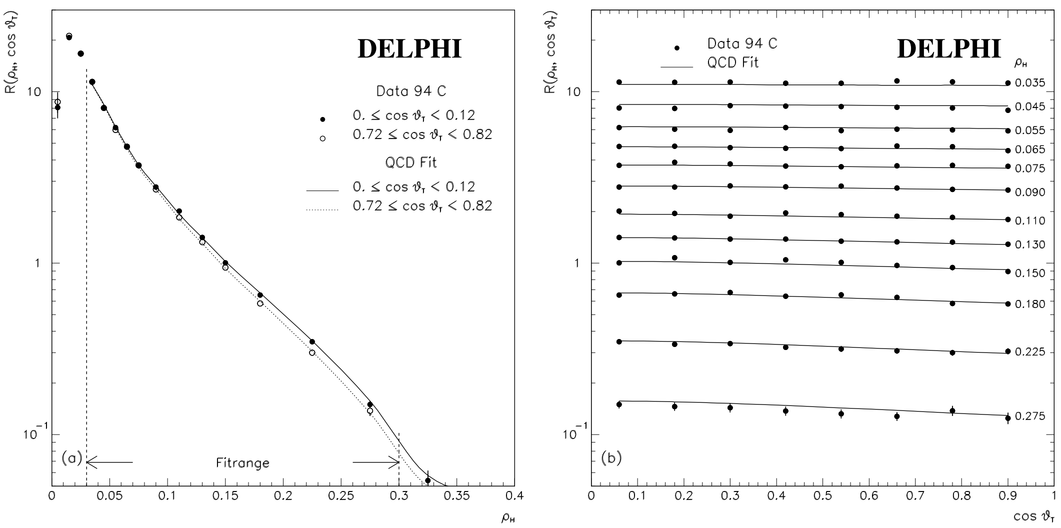

Figure 7: Same as figure 6 but for the heavy jet mass ρ_H.

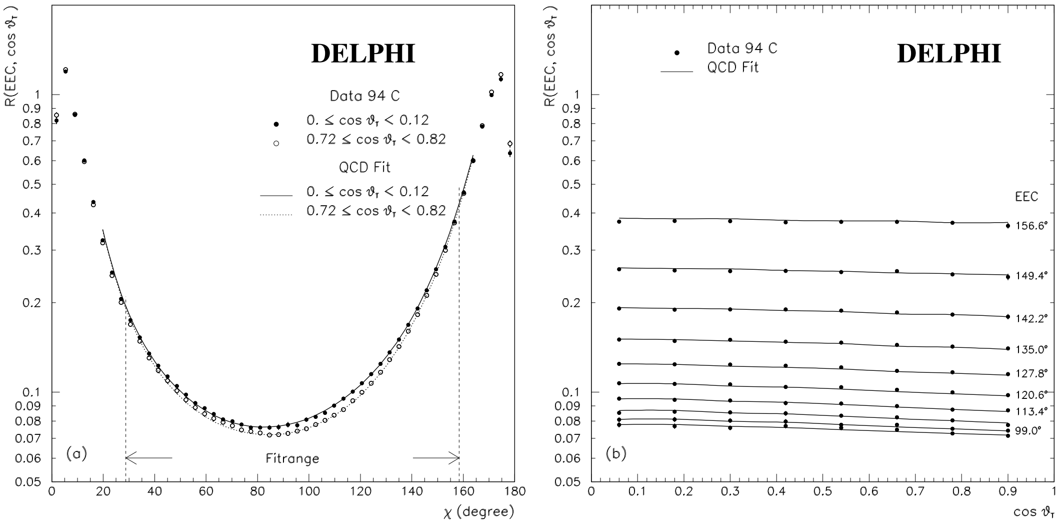

Figure 8: Same as figure 6 but for the energy energy correlation EEC.

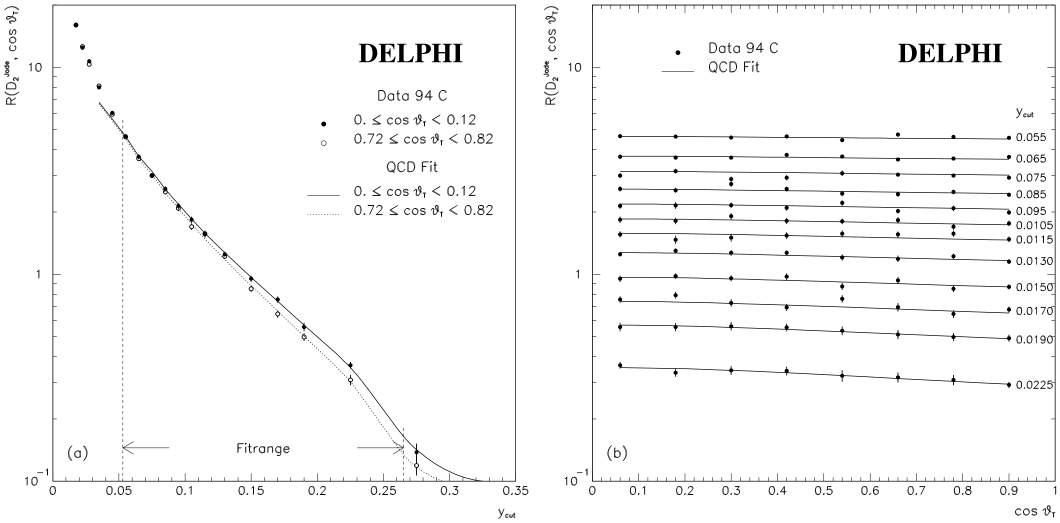

Figure 9: Same as figure 6 but for the differential two jet rate with the Jade Algorithm D_2^{Jade}.

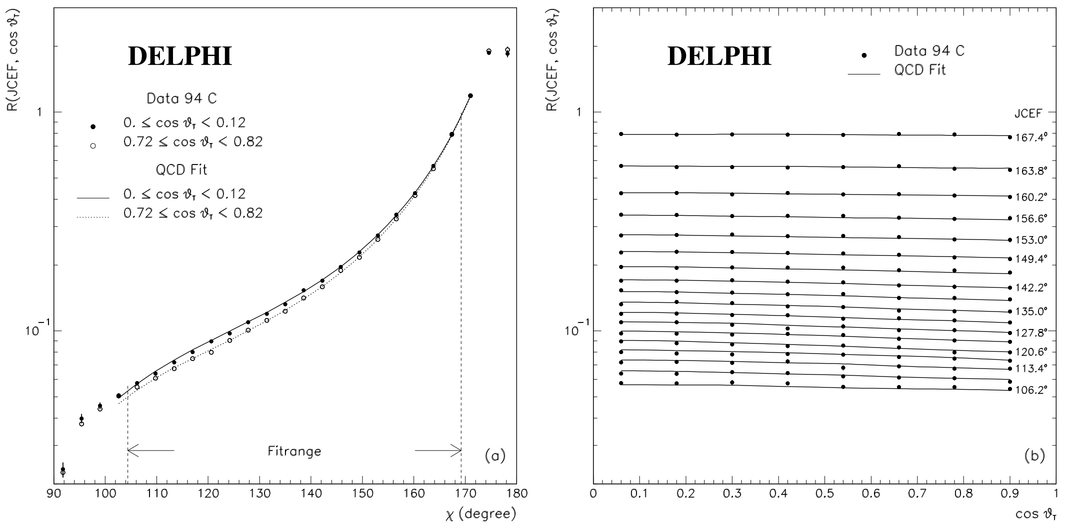

Figure 10: Same as figure 6 but for the jet cone energy fraction $JCEF$.

All combined fits on α_S and x_μ were successful with the exception of the D_2^{Geneva} observable. In this case the fit did not converge. Here x_μ was taken from a fit including charged and neutral tracks.

Combining the 15 individual results using an unweighted average yields

$$\alpha_S(M_Z^2) = 0.1165 \pm 0.0031 \ .$$

The χ^2 values, computed using the total uncertainty on the $\alpha_S(M_Z^2)$ measurements as listed in table 1 yields $\chi^2 = 8.4$, i.e. the individual measurements are fully compatible with each other within their quoted errors. The χ^2 value is significantly smaller than the number of degrees of freedom, indicating that there is a high, intrinsic correlation between the 15 observables.

The idea behind the common analysis of such a large number of observables is to optimize the use of the information contained in the complex structure of multi-hadron events. Errors due to the corrections for hadronization effects may be expected to cancel to some extent in the averaging procedure. To test this expectation the analysis of each of the individual 15 observables is repeated by performing hadronization corrections with all hadronization generators described in section 3.2. This results in 7 times 15 individual α_S values. As a first test for each of the 15 observables the unweighted average value of α_S from the seven models is evaluated. The average value of the 15 α_S values is $\alpha_S(M_Z^2)$ $= 0.1168 \pm 0.0031$. In a second step for each of the 7 hadronization models an unweighted average of the corresponding 15 α_S values is calculated. Finally an unweighted average of the 7 average values for each hadronization models is computed resulting in $\alpha_S(M_Z^2)$ $= 0.1169 \pm 0.0018$. The result confirmes that the scatter of the average values due to different assumptions for hadronization corrections is significantly smaller than the uncertainty of ± 0.0031 of the mean value from 15 individual observables.

In order to calculate a weighted average for the observables one has to take into account the correlations between the observables. Since the correlations are mostly unknown, the exact correlation pattern is hardly to work out reliably. Therefore in a first approach, we use a recently proposed simple method [24], which makes use of a robust estimation of the covariance matrix for a conservative estimation of the correlated errors. Here it is assumed, that different measurements i and j are correlated with a fixed fraction ρ_{eff} of the maximum possible correlation C_{ij}^{max}:

$$C_{ij} = \rho_{eff} C_{ij}^{max} \quad i \neq j, \quad \text{with} \quad C_{ij}^{max} = \sigma_i \sigma_j \tag{35}$$

For $\rho_{eff} = 0$ the measurements are treated as uncorrelated, for $\rho_{eff} = 1$ as 100 % correlated entities. The value ρ_{eff} then is adjusted such that the χ^2 is equal to the number of degrees of freedom n_{df}:

$$\chi^2(\rho_{eff}) = \sum_{i,j} (x_i - \overline{x})(x_j - \overline{x})(C^{-1})_{ij} = n - 1 = n_{df} \tag{36}$$

Applying this method to 14 observables (ρ_D is related to ρ_H and ρ_S by Eq. (9)) our final result is

$$\alpha_S(M_Z^2) = 0.1164 \pm 0.0021,$$

fully compatible with the world average $\alpha_S(M_Z^2) = 0.118 \pm 0.003$ and in particular with recent calculations from lattice gauge theories [25]. Figure 11 shows again the result of the weighted average for the 14 correlated observables compared to the results for the individual distributions.

6 Summary

From 1.4 Million hadronic Z_0 decays recorded with the DELPHI detector and reprocessed with improved analysis software the distributions of 15 infrared and collinear safe observables have been precisely measured at various values of the polar angle ϑ_T of the thrust axis with respect to the beam direction. In order to compare with QCD calculations in $\mathcal{O}(\alpha_s^2)$, hadronization corrections to the data are evaluated from recently tuned fragmentation models. Fits taking explicit account of the event orientation to all data points with experimental acceptance corrections less than $\sim 25\%$ and hadronization corrections less than $\sim 40\%$ yield the surprising result that the highly precise data can be accurately described by using a common value of $\alpha_S(M_Z^2)$ inside a very small error: $\alpha_S(M_Z^2) = 0.1165 \pm 0.0031$. Therefore this analysis provides a detailed and transparent test of $\mathcal{O}(\alpha_s^2)$ QCD.

Consistency of the 15 individual $\alpha_S(M_Z^2)$ determinations from the 15 shape distributions is achieved by using the different values of the renormalization scales as obtained from the individual fits within their errors, i.e. the so-called experimental optimization method is applied. It should be noted that the good agreement is achieved without any

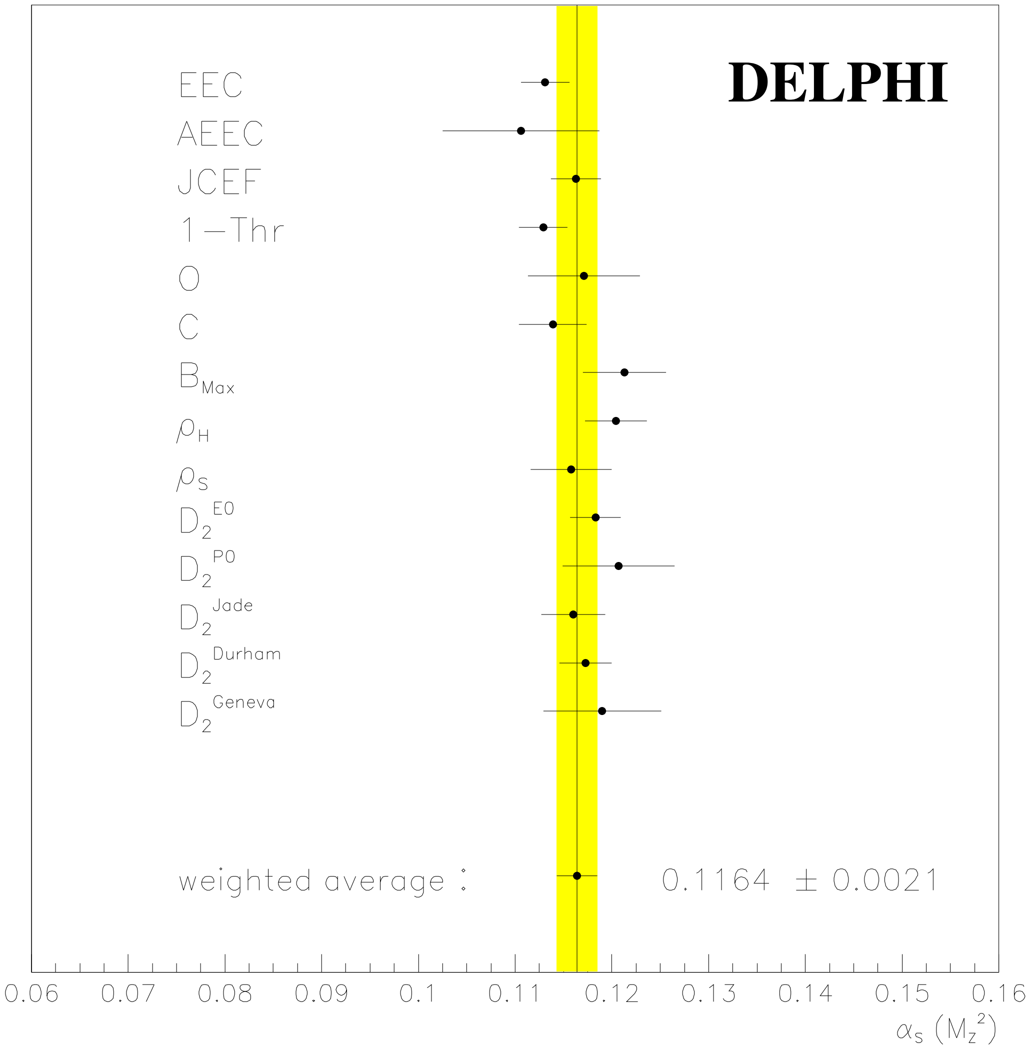

Figure 11: Results of the fits of 14 event shape distributions together with their weighted average. ρ_D has been excluded from the averaging procedure, since it is fully correlated with the other two jetmass observables ρ_H and ρ_S.

artificial increase of the renormalization scale errors. Taking full account of the correlations between the observables an average of

$$\alpha_S(M_Z^2) = 0.1164 \pm 0.0021$$

can be derived. The quoted error includes statistical and experimental uncertainties as well as uncertainties due to hadronization corrections and uncertainties of the values of the individual renormalization scales resulting from the fits. In an earlier publication of the DELPHI Collaboration an additional renormalization scale error of $\pm$ 0.006 has been quoted which was expected to also include the uncertainties of second order perturbation theory. The updated analysis shows that this error is too large. An attempt to update the evaluation of this uncertainty is in progress.

Acknowledgements

We thank M. Seymour for providing us with the EVENT2 generator and for useful discussions. We further thank P. Zerwas ... for critical comments and stimulating discussions.

References

[1] S. Catani and M. Seymour, Nucl. Phys. B485(1997) 291-419.

[2] program EVENT2, M. Seymour, URL: http://suryal1.cern.ch/users/seymour/nlo.

[3] DELPHI Collab., P. Abreu et al., Z. Phys. C59 (1993) 21.
DELPHI Collab., P. Abreu et al., Z. Phys. C52 (1991) 271.

[4] DELPHI Collab., P. Abreu et al., Z. Phys. C73 (1996) 11.

[5] K. Hamacher and M. Weierstall, DELPHI Note, DELPHI 95-80 PHYYS 515 (1995)

[6] DELPHI Coll., P. Abreu et al., Nucl. Inst. and Meth. A378 (1996) 57

[7] F. Jadach, B.F.L. Ward, Z. Was, Comp. Phys. Comm. 40 (1986) 285.
Nucl. Phys. B253 (1985) 441.

[8] T. Sjöstrand, Comp. Phys. Comm. 39 (1986) 347.
T. Sjöstrand and M. Bengtsson, Comp. Phys. Comm. 46 (1987) 367.

[9] J.E. Campagne and R. Zitoun, Z. Phys. C 43 (1989) 469.

[10] L. Lönnblad, Comp. Phys. Comm. 71 (1992) 15.

[11] G. Marchesini et al., Comp. Phys. Comm. 67 (1992) 465.

[12] P. N. Burrows, H. Masuda, Z. Phys. C63, (1994), 235-240

[13] S. J. Brodsky, G.P. Lepage, P. B. Mackenziee, Phys. Rev. D28 (1983) 228.
G. Grunberg, Phys. Rev. D29 (1984) 2315.
P. M. Stevenson, Phys. Rev. D23 (1981) 2916.

[14] G. Kramer and B. Lampe, Z. Phys. C39 (1988) 101

[15] S. Brandt et al., Phys. Lett. 12 (64) 57.
E. Fahri, Phys. Rev. Lett. 39 (1977) 1587.

[16] Mark J Collab., D. P. Barber et al., Phys. Rev. Lett. 43,830 (1979)
Mark J Collab., D. P. Barber et al., Phys. Lett. 89b, 139 (1979).

[17] R.K. Ellis, D.A. Ross, A.E. Terrano: Nucl. Phys. B178 (1981) 421.
G. Parisi: Phys. Lett. B74 (1978) 65.
J.F. Donohue, F.E. Low, S.Y. Pi: Phys. Rev. D20 (1979) 2759.

[18] S. Catani, G. Turnock and B. R. Webber, Phys. Lett. B295, 269 (1992)

[19] S. Bethge et al., Nucl. Phys. B370 (1992) 310.

[20] JADE collab., W. Bartel et al., Z. Phys. C33 (1986)
JADE collab., S. Bethge et al., Phys. Lett. B213 (1988) 235.
S. Catani and M. Seymour, Nucl. Phys. B485(1997) 291-419.

[21] N. Brown and W. J. Stirling, Phys. Lett. B252 (1990) 657
S. Bethke et al., Nucl. Phys. B370 (1992) 310.

[22] C. L. Basham et al., Phys. Rev. Lett. 41 (1978) 1585
C. L. Basham et al., Phys. Rev. D17 (1978) 2298

[23] Y. Ohnishi and H. Masuda, SLAC-PUB-6560 (1994)

[24] M. Schmelling, Phys. Scripta 51 (1995) 676.

[25] M. Schmelling, Plenary talk given at the *XXVIII International Conference on High Energy Physics* , Warsaw, July 25-31, 1996.